

Cite this: *Green Chem.*, 2022, **24**, 9552

An enhanced strategy based on the pyrolysis of bean dregs for efficient selective recovery of lithium from spent lithium-ion batteries†

Tianning Lin,^a Yue Wang,^b Shan Jin,^a Deying Mu,^a Jian Zhang,^b Jianquan Liang^b and Changsong Dai *^a

With the vigorous development of the lithium-ion battery (LIB) industry, the scarcity and non-renewability of lithium resources mean that the efficient selective recovery of Li from the spent LIBs turns progressively essential. Herein, by utilizing bean dregs (BDs) as a green reducing agent, an enhanced recycling strategy combining biomass reduction roasting and carbonated water leaching was explored. During the roasting process, the pyrolysis of BDs promoted the decomposition of the cathode material and converted it into Ni, Co, MnO, and Li₂CO₃. According to the thermodynamic analysis and the physical characterization of roasted products, a lattice collapse model was exploited to illuminate the thermochemical reaction mechanisms under the synergistic reduction effect of gases and biochar. Moreover, the parameters of the carbonated water leaching process were optimized by the response surface method (RSM) and the central composite design (CCD), and the leaching rate of Li was further enhanced. Economic assessment results indicate that this recycling strategy enhances the total profits by reducing energy and reagent consumption and increasing the recovery efficiency of Li. Overall, based on the pyrolysis of BDs, the enhanced strategy provides new perspectives and expectations for the future spent LIB recycling industry.

Received 12th September 2022,
Accepted 11th November 2022

DOI: 10.1039/d2gc03439e

rsc.li/greenchem

Introduction

Owing to high energy density, low self-discharge, and long life, lithium-ion batteries (LIBs) have become the predominant power source (>80%) in consumer electronics.^{1,2} With the ever-increasing popularity of electric vehicles (EVs), the demand and production of LIBs in the automotive industry will explode globally in the next few years, and the EV market is expected to reach 26 951 318 units in 2030, according to a report by the International Energy Agency.^{3,4} Nonetheless, the performance of these LIBs commonly degrades after 1000 cycles, meaning that their average lifespan rarely exceeds 5 years, which will generate a great deal of spent LIBs.^{5,6} Since the contents of metals such as Li, Ni, Co, and Mn are more abundant than these of natural ores, spent LIBs have turned into a vital secondary resource, namely “urban mines”.⁷ Hence, it is remarkably crucial to carry out

a recycling strategy with high efficiency and low environmental footprint for the sustainable development of the LIB industry.⁸

The typical strategies for recycling spent LIBs are based on hydrometallurgy or pyrometallurgy.^{9,10} Above all, hydrometallurgy is acknowledged as the most promising recycling strategy due to its high leaching efficiency,¹¹ high metal selectivity,¹² and distinguished product purity.¹³ Even so, in hydrometallurgical recycling processes, the residual liquid obtained after the separation of valuable metals holds a low Li content (<2 g L⁻¹), and a lot of difficult-to-separate Na⁺/NH₄⁺ impurities (~5 g L⁻¹).^{14,15} Only about 70% Li could be recovered economically from the residual liquid. For pyrometallurgical recycling methods, spent LIBs are recovered in the form of metals or alloys by employing a high-temperature smelting furnace, which retains the advantages of high chemical reaction rate,¹⁶ simple operation,¹⁷ and effectively separating metal elements.¹⁸ In spite of these, Li is frequently lost as a by-product in the slag or evaporated during high temperature treatments, which leads to a low Li recovery rate.^{19,20} Obviously, with the robust development of the LIB industry, it is foreseeable that over the next decade, the world will face severe Li shortages due to the scarcity and non-renewability of Li ore resources.²¹ To avoid this supply crisis, at least 90 wt% of Li in the spent LIBs needs to be recycled.^{22–25} However, the recovery efficiencies of Li

^aMIIT Key Laboratory of Critical Materials Technology for New Energy Conversion and Storage, School of Chemistry and Chemical Engineering, Harbin Institute of Technology, Harbin 150001, P.R. China. E-mail: changsd@hit.edu.cn

^bElectric Power Research Institute, State Grid Heilongjiang Electric Power Co., Ltd, Harbin, 150030, P. R. China

† Electronic supplementary information (ESI) available. See DOI: <https://doi.org/10.1039/d2gc03439e>

obtained by the current recovery strategies are still at a low level, and further improvements must be achieved.

In order to enhance the recovery efficiency of Li, researchers have developed the recovery strategies combined with hydrometallurgy and pyrometallurgy, such as the recycling methods integrated carbothermal reduction and water leaching, which are capable of reducing energy consumption and selectively recycling Li with high efficiency.^{26–29} For instance, Tang *et al.* mixed spent LiCoO₂ with graphite for carbothermal reduction and then selectively extracted Li₂CO₃ by water leaching.³⁰ Zhao *et al.* utilized microwave heating to promote the carbothermal reduction of cathode materials with anthracite, so cathode materials were rapidly reduced and the recovery of Li₂CO₃ was achieved by water leaching.³¹ As a renewable,³² non-polluting,³³ and carbon-balanced resource,³⁴ waste biomass has attracted more and more attention in thermochemical processes, and has been considered to be an excellent solution to alleviate the energy crisis and get rid of fossil fuel dependency.^{35,36} Recently, Zhou *et al.* reported a biomass carbothermal reduction approach to recover metal resources from spent LiCoO₂ by pine sawdust.³⁷ Chen *et al.* probed different biomass wastes as reductants for selective leaching of Li from spent LIBs, and the corn stalk exhibited the best reducing capacity among the others.³⁸ As we all know, bean dreg (BD) is the main by-product in the processing of soybean products, and China, where soybeans are the main oil crops and food resources, produces up to 80 000 tons of BD waste every year.³⁹ Therefore, the collection and availability of BDs for further application overcome many other kinds of biomass which have a relatively low output or regional limitation, while only a small fraction of BDs is used as feed for livestock, and most of them are not fully exploited. In recent years, based on the benefits of energy conservation and environmental protection, BDs have been utilized as a source of renewable energy or value-added products, such as ammonia nitrogen removal⁴⁰ and preparation of hierarchical porous carbon.⁴¹ To the best of our knowledge, the application of BDs has not been reported in the field of spent lithium-ion battery recycling. Therefore, it is of great significance to in-depth explore the thermochemical behaviors and the reaction mechanisms in the roasting process of BDs as a green reducing agent and enhance the recovery process for the realization of high-efficiency lithium selective recovery.

Herein, for the purpose of achieving high-efficiency and low-environmental footprint recycling of spent LIBs, we exploited bean dregs as a green reducing agent, and adopted an enhanced recycling process combining biomass reduction roasting and carbonated water leaching to selectively recover Li from the spent LIBs. The thermodynamic data of related chemical reactions of the LiNi_{0.5}Co_{0.2}Mn_{0.3}O₂ (NCM-523) decomposition and the BDs pyrolysis products were calculated and analyzed by HSC software. Based on the detailed characterization by TG-DSC-MS, SEM, XRD, and XPS, the material transformation and thermochemical reaction mechanisms during the roasting process were explored. In addition, the synergistic reduction effect of gases and biochar was investi-

gated by independent experiments. The effects of the roasting temperature, dosage ratio, and roasting time on the leaching rate of Li were explored to optimize the roasting conditions. Simultaneously, the variables of carbonated water leaching (time, CO₂ flow rate, temperature, and solid-liquid ratio) were optimized by RSM and CCD methods to enhance the recycling process, and obtained a global optimal solution for the maximum leaching rate of Li. Finally, through the calculation and analysis of practical application capability and recycling benefits, it is verified that the enhanced recycling strategy in this paper will demonstrate great development potential in the future LIB recycling industry.

Materials and methods

Materials

Bean dreg (BD) is the common waste produced during soymilk production in breakfast shops or soy product factories. Being free from impurities and tiny particles greatly reduces the difficulty of employing BDs as a reducing agent, and then reduces a part of the labor costs in future industrial applications. In this work, BDs were thoroughly soaked and washed 3 times with deionized water to remove impurities, and then dried in a vacuum oven (110 °C) overnight.^{39,42} The elemental contents of BDs were determined using an organic element analyzer. The detailed composition is illustrated in Table S1.† The spent cathode material LiNi_{0.5}Co_{0.2}Mn_{0.3}O₂ (SNCM-523) used in this research was sourced from a battery recycling plant collaborating with our research group. Fig. S1 in the ESI† shows the pre-treatment process. SNCM-523 was digested in aqua regia for 3 h and the contents of Li, Ni, Co, Mn, Al, and Cu were tested by inductively coupled plasma optical emission spectrometry (ICP-OES) and are shown in Table S2.† In addition, other spent LIB cathode materials including lithium cobalt oxide (LCO) and lithium manganese oxide (LMO) were acquired by the same preparation process. The scanning electron microscopy (SEM) images and the X-ray diffraction (XRD) patterns of the obtained SNCM-523 cathode material are shown in Fig. S2 and S3.† All the chemicals (H₂SO₄, HNO₃, and HCl) were of analytical grade and purchased from Sigma Aldrich Co. Ltd, and deionized water was used for carbonated water leaching, aqueous solution preparation, and washing.

Experimental procedure

Biomass reduction roasting. A schematic diagram of the recycling process is shown in Fig. 1. A certain amount of SNCM-523 and BDs was ground in an agate mortar for 10 min to ensure that the reactants were uniformly mixed and transferred to a tube furnace (OTF-1200X, HF-Kejing) for roasting under high-purity Argon (Ar) atmosphere (100 mL min⁻¹). The dosage ratios of SNCM-523 and BDs were 1:0.1–1:2. The temperature range was 500–800 °C with a heating rate of 10 °C min⁻¹, and the holding time was in the range of 20–180 min. After the roasting process, the obtained samples were ground in an agate mortar again for 5 minutes before the subsequent

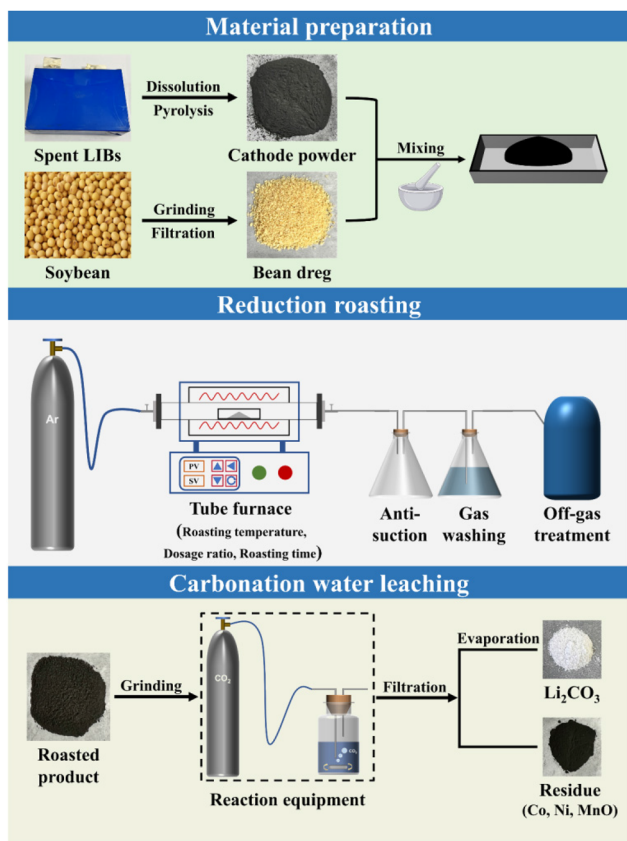


Fig. 1 Schematic diagram of the enhanced recycling process.

characterization and separation procedures. Part of the powders was dissolved in aqua regia to test the Li, Ni, Co, and Mn concentrations by ICP-OES. The effects of roasting temperature, dosage ratio, and roasting time on the leaching rate of Li were investigated.

Carbonated water leaching. Carbonated water leaching was performed in a 1 L wild-mouth bottle reactor on a magnetic stirrer with heating equipment. A certain amount of roasted powder and deionized water was introduced into the reactor, and a CO₂ cylinder with a flow meter was equipped. During the leaching process, the flow meter was controlled at a constant flow rate, while stirring the solution at a speed of 400 rpm and the temperature was kept constant by means of heating equipment. After a certain leaching time, the solution was filtered. The filtrate was heated to 100 °C in a 500 mL glass beaker to recover Li₂CO₃ and held the temperature until approximately 80% water had evaporated. Subsequently, the suspension was filtered, and the obtained white powder was washed with boiling deionized water and dried for 12 h. Afterward, XRD and SEM were performed to characterize the recycled Li₂CO₃ powder. Moreover, a part of the filtrate was taken for ICP-OES tests to determine the leaching rate of Li.

Calculations and analytical methods

Response surface methodology to optimize carbonated water leaching. A more accurate analysis of process behaviour

may be possible by using a different experimental design approach.⁴³ Among these methods, the RSM is preferable due to its high accuracy and efficiency.⁴⁴ The optimal operating variables of the experimental process can be determined through the analytical regression equation of the RSM, and the corresponding physical and mathematical models can be provided for the practical application of the relevant process, thereby realizing the optimization of the process conditions.^{45–47} In this study, the CCD was used to investigate the optimal level points of each factor in the carbonated water leaching experiment, and the RSM was exploited to analyse the results. The variables selected in this study were time (h), CO₂ flow rate (mL min⁻¹), temperature (°C), and solid-liquid ratio (g L⁻¹).

The behaviour of the system can be analysed using eqn (1).⁴⁸

$$Y = \beta_0 + \sum \beta_i X_i + \sum \beta_{ii} X_i^2 + \sum \beta_{ij} X_i X_j + \varepsilon (i < j) \quad (1)$$

Here Y is the model prediction that depends on the independent variable (the leaching rate of Li); β_0 is a constant which can be positive or negative, and β_i ($i, j = 1, 2, \dots, k$) is the coefficient of the linear variable expected to be significant for the primary variable in the design, which can be assessed by the p -value obtained from analysis of variance (ANOVA). β_{ii} is a coefficient describing the magnitude of the nonlinear parameter. As for β_{ij} ($i, j = 1, 2, \dots, k$), if it is significant, it indicates the interaction between variables. ε is the error term, which is the same component that causes the model predictions to differ slightly from the actual results.

The leaching rate of Li (R_{Li}) is defined as follows:

$$R_{Li} = \frac{C_{Li} V}{m_0 w_0} \times 100\% \quad (2)$$

where m_0 (g) and w_0 (%) are the mass of the cathode material and the weight content of element “Li” in it, C_{Li} (g L⁻¹) and V (L) are the concentration of element “Li” and the volume of the leaching solution, respectively.

And the recovery efficiency of transition metal (R_i) is defined as follows:

$$R_i = \frac{M_i}{M_p} \times 100\% \quad (3)$$

where M_i is the moles of transition metal “i” in the carbonated water leaching product, and M_p is the moles of the element in the mixed powders.

The “Design Expert 12.0” software was applied to calculate the coefficients of the analytical fit equation and to perform statistical analysis on the response surface model. The best fit of the model was obtained by comparing the model predicted value with the experimental value and the best combination was obtained by response surface analysis. Simultaneously, so as to validate the experimental results and the model results derived from the statistical experiments, all experiments were repeated 3 times to obtain the average data of the leaching rate of Li.

Analytical methods. The contents of metal elements (such as Li, Ni, Co, Mn, Cu, and Al) and the concentrations of Li were determined by utilizing inductively coupled plasma optical emission spectrometry (ICP-OES, ICAP 7400, Germany). The elemental contents of BDs were determined by exploiting an organic element analyzer (Elementar, Germany). The surface morphology, crystal structures, and chemical compositions of spent cathode materials, roasted samples, and carbonated water leaching residues were characterized by scanning electron microscope (SEM, HITACHI, S-4700, Japan), X-ray diffraction (XRD, Rigaku, Japan), and X-ray Photoelectron Spectroscopy (XPS, PHI5700 ESCA, USA). A thermogravimetric analyzer (TG/DSC, NETZSCH, STA449F3, Germany) was exploited to reveal the thermochemical properties and behaviors during the roasting processes, applying about 5–10 mg of homogeneously mixed samples (dosage ratio of SNCM-523 : BDs is 1 : 0.3), heated from room temperature to 1000 °C, a heating rate of 10 °C min⁻¹ under a high-purity N₂ atmosphere. The gas properties were characterized by combining the thermogravimetric analyzer with a mass spectrometer (MS, NETZSCH, QMS403D, Germany) during the TG-DSC testing processes. The Gibbs free energies of the relevant chemical reactions were calculated using HSC Chemistry 9.0 software.

Results and discussion

Thermodynamic and thermogravimetric analysis

The thermodynamic data are able to reflect the occurrence probability of relevant chemical reactions, energy conversion, and phase transition. During the roasting process, both the reducing gases and biochar, generated from the pyrolysis of BDs, can react with the decomposition products of SNCM-523. Therefore, the reduction process is divided into two main parts, gas reduction and carbothermal reduction. Herein, based on the roasting process, the thermodynamics of the corresponding reactions were explored. The relationships between the temperatures and standard Gibbs free energies were analysed to evaluate whether the reactions proceeded spontaneously, and compare which reactions are thermodynamically favorable. However, the reactants are always not in the corresponding standard states, and therefore, the Gibbs free energies of the corresponding reactions derived from the isotherm equation are expressed as:³⁷

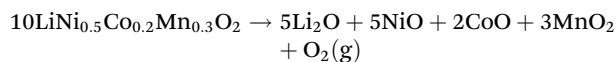
$$\Delta_r G_m(T) = \Delta_r G_m^\theta(T) + RT \ln Q \quad (4)$$

where $\Delta_r G_m(T)$ and $\Delta_r G_m^\theta(T)$ are the Gibbs free energy (kJ) and the standard Gibbs free energy (kJ) at T , respectively; R is the molar gas constant, 8.314 J mol⁻¹ K⁻¹; T is the thermodynamic temperature (K), Q is the reaction quotient. When a reaction reaches its equilibrium state, $\Delta_r G_m(T) = 0$ or $\Delta_r G_m^\theta(T) = -RT \ln Q$; otherwise, $\Delta_r G_m(T) < 0$ indicates that the chemical reaction can proceed spontaneously and *vice versa*.

First of all, just like the reaction formula listed below, LiNi_{0.5}Co_{0.2}Mn_{0.3}O₂ will decompose into NiO, CoO, Li₂O, MnO₂, and O₂. Then, the reducing gases (such as H₂, CH₄,

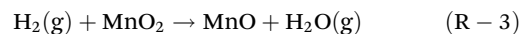
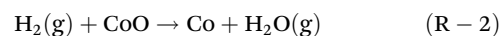
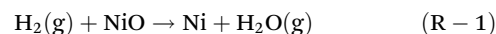
NH₃, and CO) and biochar from the pyrolysis of BDs will undergo reduction reactions with the LiNi_{0.5}Co_{0.2}Mn_{0.3}O₂ decomposition products, respectively. It is worth noting that the thermal decomposition of the peptide bonds in the protein structure of BDs will release the strongly reducing NH₃. The protein content of BDs accounts for more than 20%,⁴² so a large amount of NH₃ will be generated. At this point, the basic reaction process between BDs and NCM-523 can be divided into the following steps:

Pyrolysis of LiNi_{0.5}Co_{0.2}Mn_{0.3}O₂:

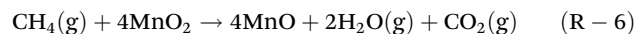
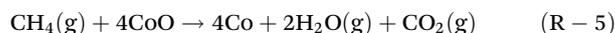
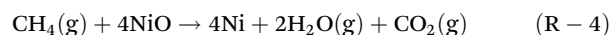


Gas thermal reduction:

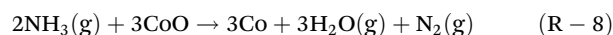
(1) Thermal reduction of H₂;



(2) Thermal reduction of CH₄;



(3) Thermal reduction of NH₃;



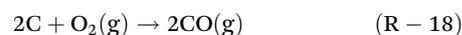
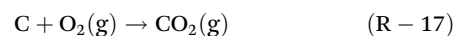
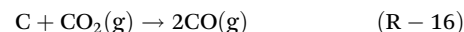
(4) Thermal reduction of CO;



Biochar thermal reduction:



Combustion reaction of carbon:



Reaction of CO₂ with Li₂O:



Based on the above reactions, the relationships between the calculated Gibbs free energies ($\Delta_r G_m(T)$) and the temperatures are shown in Fig. 2. The reaction formulas of MnO with reducing gases and biochar and the detailed Gibbs free energy calculation results are shown in Fig. S4.† Whether MnO reacts with gases or biochar, the Gibbs free energies of the reactions are all greater than 0, indicating that these reactions are all non-spontaneous. As shown in Fig. 2a–d, the Gibbs free energies of the gas reduction reactions ((R-1)→(R-12)) are all negative across the entire temperature range, indicating that the gas reduction reactions tend to proceed at low temperatures. By comparing Fig. 2a–d with 2e, the biochar reduction reactions ((R-13), (R-14), and (R-15)) have higher initial reaction temperatures than the gas reduction reactions. Furthermore, in the gas reduction reactions (Fig. 2a–d), the Gibbs free energies of CH₄ and NH₃ reactions ((R-4)→(R-9)) are lower than those of H₂ and CO ((R-1), (R-2), (R-3), (R-10), (R-11), and (R-12)), and in terms of thermodynamics, the decomposition products of NCM-523 will be preferentially reduced by them. Hence, compared with traditional aluminothermic reduction and carbothermal reduction, the exploitation of BDs as the green reducing agent is of great significance for reducing the reaction temperature and energy consumption. Finally, due to the negative Gibbs free energy (R-19), Li₂O will interact with CO₂ to form Li₂CO₃.

Fig. 2g and h shows the TG-DTG-DSC curves for the roasting of BDs alone and the mixed sample of BDs and NCM-523. The DTG curve is the first derivative curve of the TG curve

reflecting the weight loss rate of the roasted sample. In the TG curve of Fig. 2g, the BDs have a small weight loss in the temperature range of 80–179 °C and the DSC curve shows an endothermic peak, which is caused by the escape of free and bound water in the BDs during roasting. When the temperature exceeds 179 °C, the main mass loss stage of BDs appears around 569 °C, and the loss ratio reaches 77.43%. Meanwhile, the DSC curve demonstrates that there are three endothermic peaks (peak 1, 2, and 3) in this temperature region, indicating that the pyrolysis of BDs into gas, biochar, and bio-oil is responsible for the most of the mass loss. In order to characterize the pyrolysis gas properties, the roasting process was tested by combining mass spectroscopy and TG-DSC (TG-DSC-MS), and the corresponding mass spectra are presented in Fig. S5.† It can be spotted from Fig. S5a† that the main gases produced during the BDs pyrolysis process are H₂, CH₄, NH₃, and CO. Due to the extraordinary protein content in BDs, the mass spectrum intensity of NH₃ is the highest among the others.⁴² Furthermore, in Fig. S5b–e,† the peak temperatures of reducing gases in the mass spectra are very close to the temperature of the maximum mass loss rate in the DTG curve, indicating that a large amount of reducing gases are produced in this temperature range. After this stage, C–C and C–H bonds in the BDs were largely broken with the increasing pyrolysis degree, and the most volatile substances were converted to gases. Meanwhile, non-volatile substances (mainly biochar) were left in the roasted products.

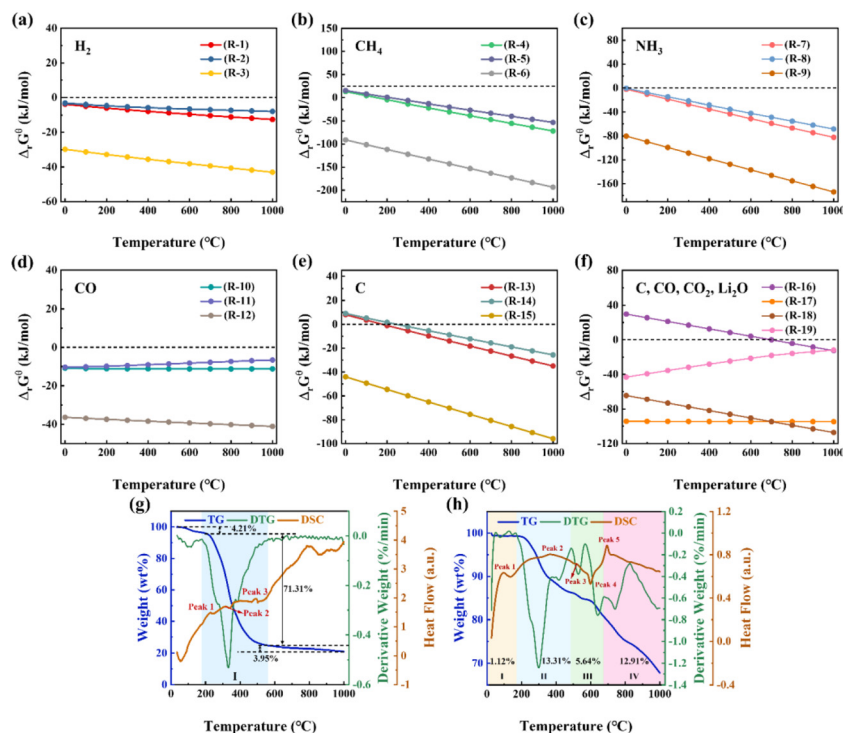


Fig. 2 Schematic diagrams of the relationships between the Gibbs free energies and temperatures for the chemical reactions during the reduction roasting process: (a) H₂ reduction, (b) CH₄ reduction, (c) NH₃ reduction, (d) CO reduction, (e) carbothermal reduction, (f) reactions of C, CO, O₂, and Li₂O; TG-DTG-DSC curves of (g) BDs and (h) the mixed sample of BDs and NCM-523 (dosage ratio: 1 : 0.3) under an Ar atmosphere (temperature range: 30–1000 °C, heating rate: 10 °C min⁻¹).

The main weight loss of the mixed sample (dosage ratio of BDs and NCM-523 is 1 : 0.3) in the TG curve is mostly concentrated in the four temperature ranges of 30–172 °C, 172–488 °C, 488–677 °C, and 677–1000 °C in Fig. 2h, while the mass loss in the range of 172–488 °C reaches 13.31%, which is the largest among the four stages. At stage II, the mass loss curve of the mixed sample is similar to the TG curve of BDs, indicating that the volatilization of BDs pyrolysis gases is still the main cause. However, from Fig. 2h, the endothermic peak (peak 2) temperature in the DSC curve is a little higher than the temperature of the maximum weight loss rate, which indicates that the pyrolysis gases (H_2 , CH_4 , NH_3 , and CO) undergo pre-reduction reactions with the decomposition products (NiO , CoO , and MnO_2) during stage two. To verify this phenomenon, referring to Fig. 2a–d, in this temperature range, the thermodynamic conditions for the pyrolysis gas reduction reactions of metal oxides have been completely reached (the Gibbs free energies of (R-1)–(R-12) are all negative), demonstrating that these reactions can all proceed spontaneously. It is worth noting that the decomposition of the cathode powder can be promoted by the coupled reaction when the pyrolysis gases start to react with the decomposition products.⁴⁹ As shown in Fig. S6,† TG-DSC-MS was also applied to characterize the gas properties generated during the roasting process of the mixed sample. Among them, the temperatures corresponding to the maximum intensities of H_2 , CH_4 , and NH_3 are similar to the peak temperature of the DTG curve (300 °C), and the intensity begins to decrease after this temperature, indicating that the gas reduction reaction has occurred, which also proves the pre-reduction phenomenon. From stage three, the pyrolysis gases of BDs and the decomposition products of NCM-523 start to react violently. There is an exothermic peak (peak 4) around 600 °C in the DSC curve, which represents the reduction reactions between the pyrolysis gases and transition metal oxides. Compared with stage four, the smaller temperature range and lower reaction temperature of stage three denote that the gas reduction reactions can accelerate the reduction reaction kinetics and reduce the roasting temperature. In the fourth stage, biochar further reduces transition metal oxides to Ni , Co , and MnO , and simultaneously, Li_2O will combine with CO_2 to form Li_2CO_3 . Furthermore, there is an endothermic peak (peak 5) in the DSC curve at 695 °C, demonstrating that the carbothermal reduction reactions occur around this temperature. After stage IV, due to the higher temperature, the Li_2CO_3 will gradually decompose or evaporate and the “Boudouard reaction” ($C + CO_2 = 2CO$) will occur, resulting in a faster mass loss. The same conclusion can be drawn from the mass spectrum of CO_2 (Fig. S6f†). When the temperature exceeds 600 °C, the intensity of CO_2 begins to increase, and there are two peaks at 717.4 and 879.7 °C, indicating that the carbothermal reduction continues to occur. After 879.7 °C, the decreased intensity of CO_2 verifies the existence of the “Boudouard reaction”. Ultimately, during the entire roasting process, as displayed in the mass spectra of NO , NO_2 , and CO_2 (Fig. S7†), no NO or NO_2 are produced, while CO_2 , as the main component of the tail gas, can be returned to the reactor or applied in the sub-

sequent carbonated water leaching process during the industry recycling process. This suggests that the biomass roasting process is almost not harmful to the environment.

Optimization of biomass reduction roasting

According to the above thermodynamic and thermogravimetric analysis results, it can be deduced that the pyrolysis of BDs can promote the decomposition of NCM-523 and convert the decomposition products into different products, mainly Ni , Co , MnO , and Li_2CO_3 (XRD pattern of the roasted products is shown in Fig. S8†). Therefore, so as to optimize the roasting process, the effects of roasting temperature, dosage ratio, and roasting time on the leaching rate of Li and the chemical compositions of the roasted products were investigated.

Effect of roasting temperature on the leaching rate of Li . The roasting temperature has a significant effect on the leaching rate of Li . Under the conditions of the dosage ratio of 1 : 0.5 and the roasting time of 1 h, the relationship between the roasting temperature and leaching rate of Li is shown in Fig. 3a. At around 500 °C, the leaching rate of Li is at a low level (82.41%), because the roasting process has just entered the gas reduction stage (stage 3), and most transition metal oxides have not fully reacted and Li_2O will be mantled by them, making it difficult to recover. The same consequence can also be obtained from the XRD pattern, in Fig. 3d, the peaks of roasted products consist of not only Ni , Co , and MnO , but also unreacted NiO and CoO . Since the kinetics of the MnO_2 gas reduction reaction are faster (the Gibbs free energies are smaller than the reactions of NiO and CoO), no peak of MnO_2 appears. After 500 °C, the leaching rate of Li increased significantly, and reached the maximum value at 700 °C (93.08%). At this temperature, the roasting process passes through the gas reduction stage and just enters the carbothermal reduction stage, where the transition metal oxides are all reduced and massively generated CO_2 converts Li_2O into Li_2CO_3 . It can be spotted from the XRD pattern (Fig. 3d) that there are no peaks of NiO and CoO , and the existing peaks are Li_2CO_3 , Ni , Co , and MnO at this temperature. When the roasting temperature exceeds 700 °C, the leaching rate of Li decreases, probably because Li_2CO_3 is vaporized or decomposed at such a high temperature.

Effect of the dosage ratio on the leaching rate of Li . The dosage ratio is a very vital factor in industrial production, because the amount of active substances that can be recovered in a single roasting process (the amount of sample loaded in the reactor is fixed) will affect the recovery cost and energy consumption. As shown in Fig. 3b, the reduction roasting process was carried out at 700 °C for 1 h with different dosage ratios. With the increase of dosage ratio, the leaching rate of Li also increased, and reaches the maximum value (93.59%) when the dosage ratio is 1 : 0.3. From the XRD patterns in Fig. 3e, at low dosage ratios (1 : 0.1 and 1 : 0.2), the amount of reducing gases and CO_2 is not enough, which will lead to an incomplete reduction and a decrease in the leaching rate of Li . Conversely, the leaching rate of Li declines with the dosage ratio exceeding 1 : 0.3. This is the reason that the excess biomass will generate

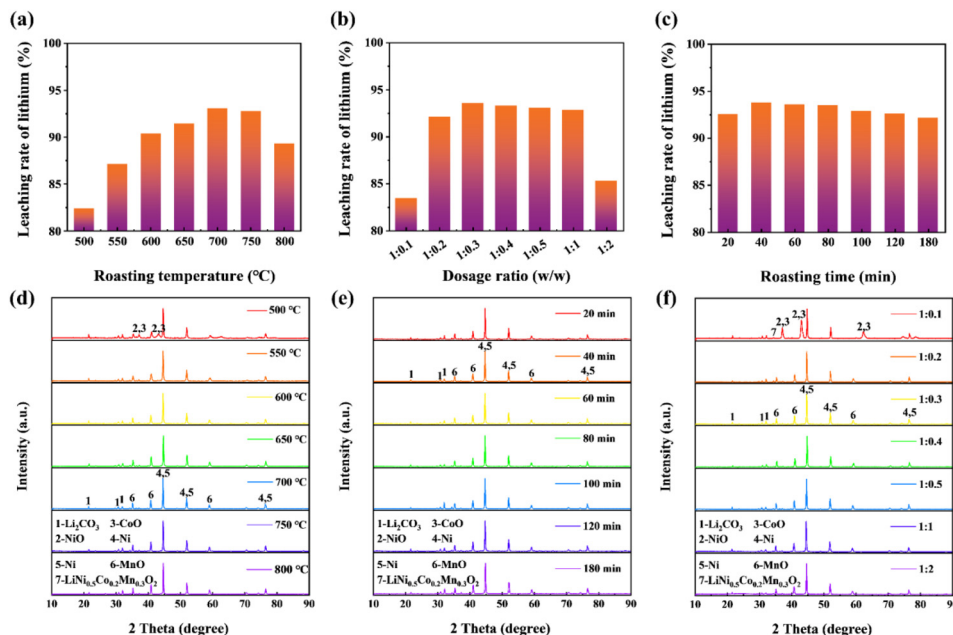


Fig. 3 Effects of (a) roasting temperature, (b) dosage ratio, (c) time on the leaching rate of Li, and (d–f) XRD patterns of the roasted products with different roasting temperatures, dosage ratios, and roasting times.

a large amount of biochar and encapsulate Li₂CO₃, forcing it to be unable to come into contact with water and CO₂ in the subsequent recycling process.

Effect of the roasting time on the leaching rate of Li. In order to explore the effect of the roasting time on the leaching rate of Li, the roasting temperature and the dosage ratio were controlled at 700 °C and 1 : 0.3. It can be clearly distinguished from Fig. 3a that with the roasting time extending from 20 min to 180 min, the differences among the leaching rates are not significant, indicating that the roasting time has little effect on the leaching rate of Li. Additionally, from the XRD patterns in Fig. 3f, the attained products do not change with the increase of roasting time, which signifies that the whole reduction process is instantaneous, and the roasting time only affects the reaction rate. Therefore, the suitable roasting time (40 min) achieves the maximum leaching rate of Li (93.78%) through the complete reduction of transition metal oxides and minimizes the loss of Li.

Synergistic reduction mechanisms of gases and biochar

The morphologies of SNCM-523, roasted products, and leaching residues were investigated by SEM and the results are displayed in Fig. S2† and Fig. 4a–h, respectively. From Fig. S2,† SNCM-523 consists of pellets of various sizes. After SNCM-523 was mixed with BDs and roasted under certain conditions, the roasted products revealed smaller particles than SNCM-523, which may be composed of Ni–Co alloys, MnO, and Li₂CO₃. Additionally, smaller particles are beneficial for the efficient recovery of Li₂CO₃ in the subsequent carbonated water leaching process. The particles of leaching residues were looser than the roasted products, and the EDS results exhibited that

the distribution of Ni, Co, and Mn elements was uniform. The XRD patterns of the roasted products and the filter residues after carbonated water leaching are displayed in Fig. 4i and j. The roasted products are composed of Ni, Co, MnO, and Li₂CO₃. For the leaching residues, due to the selective recovery of Li₂CO₃, only the peaks of Ni, Co, and MnO exist in the XRD pattern. The XPS tests were performed on SNCM-523, roasted products, and leaching residues to determine the reduction behaviors of the main elements in SNCM-523 during the roasting process and the properties of leaching residues (Fig. 5). Li 1s is present in SNCM-523 as Li–O (Fig. 5a). After the roasting process, the Li 1s spectrum is transformed into Li₂CO₃ with a characteristic peak at 54.78 eV and then there is no Li characteristic peak after the carbonated water leaching, meaning that almost all Li element is recovered in the form of Li₂CO₃.⁵⁰ For the Ni 2p spectra of SNCM-523 in Fig. 5b, the two main peaks at 854.6 eV and 872.3 eV, corresponding to Ni 2p_{3/2} and Ni 2p_{1/2} with two satellite peaks, represent Ni²⁺, and do not change after the subsequent processes. Besides, two weak peaks at 857.1 eV and 870.0 eV belong to Ni³⁺ in the SNCM-523, which disappear after the roasting process. In the Ni 2p spectra of the roasted and leaching products, the characteristic peak at 853.1 eV belongs to Ni, indicating that Ni²⁺ and Ni³⁺ are reduced to Ni by reducing gases and biochar.⁵¹ Fig. 5c displays the Co 2p spectrum of SNCM-523, and the peaks at 779.9 and 794.8 eV are consistent with Co 2p_{3/2} and Co 2p_{1/2} which are assigned to Co³⁺; furthermore, there are characteristic peaks corresponding to Co⁴⁺ at 783.6 and 796.9 eV. The binding energies of Co 2p_{3/2} and Co 2p_{1/2} of the roasted products and leaching residues change to 780.8 and 796.6 eV, matching with Co²⁺, and the characteristic peak at 778.7 eV

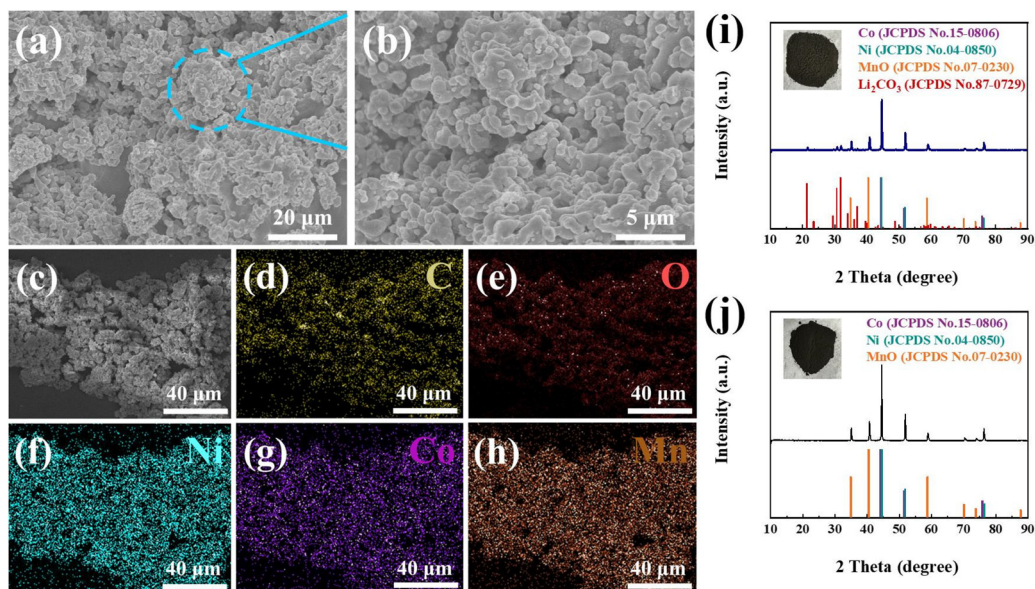


Fig. 4 SEM images of the mixed sample of BDs and NCM-523 (a and b) after roasting, (c–h) after carbonated water leaching, and XRD patterns and pictures of (i) the roasted products and (j) the filter residues after carbonated water leaching.

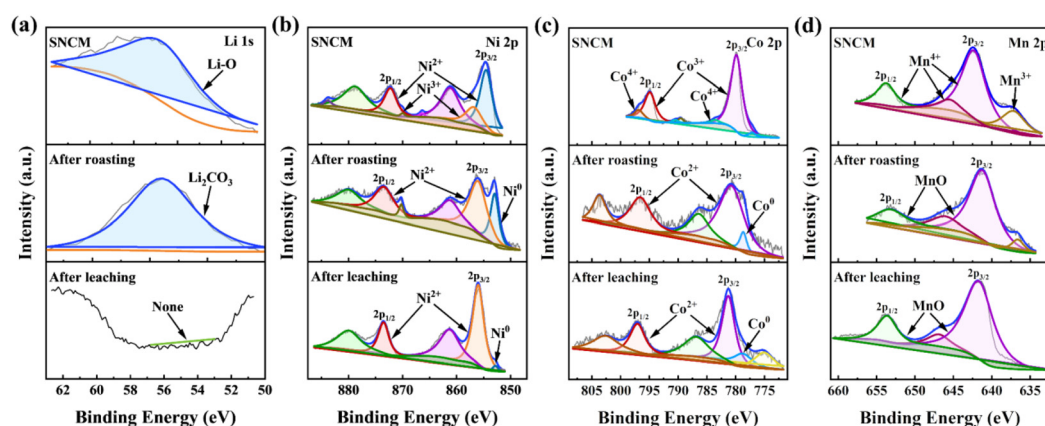


Fig. 5 High-resolution XPS spectra of (a) Li 1s, (b) Ni 2p, (c) Co 2p, and (d) Mn 2p core peaks of SNCM-523, roasted products, and leaching residues.

corresponds to Co, indicating that the Co^{4+} , Co^{3+} , and Co^{2+} were all reduced in the roasting process and did not change after the leaching process.⁵² Simultaneously, it is worth noting that there are multiple valences in the Ni 2p and Co 2p spectra of roasted and carbonated water leaching products (Fig. 5b and c), which are inconsistent with their XRD patterns (Fig. 4i and j). The reason may be that part of the Ni and Co in the roasted products are oxidized by O_2 in the air, so Ni^{2+} and Co^{2+} peaks appear in the Ni 2p and Co 2p spectra, which can be seen in previous reports.⁵⁰ And this phenomenon becomes more serious after the carbonated water leaching process (Fig. 5). The Mn 2p spectrum of SNCM-523 exhibits two characteristic peaks in Fig. 5d. Mn $2p_{3/2}$ at 642.5 eV and Mn $2p_{1/2}$ at 653.8 eV indicate that the main chemical state of Mn is Mn^{4+} , and the binding energy at 645.6 eV corresponds to the Mn^{3+} characteristic peak. After the roasting and leaching process,

the characteristic peaks of Mn $2p_{3/2}$ and Mn $2p_{1/2}$ are located at 641.6 eV and 653.4 eV, respectively, which are the binding energies of MnO. The comparison of three spectra shows that Mn^{4+} and Mn^{3+} are successfully reduced to a lower oxidation state through gas reduction and carbothermal reduction.⁵³

In an attempt to explore the thermochemical reaction mechanisms, the properties of products and the leaching rate of Li of gas and biochar reduction were investigated under the same conditions (the roasting conditions: roasting temperature of 700 °C, dosage ratio of 1:0.3, and roasting time of 40 min), respectively. The schematic diagram of the investigation process (Fig. S9†) and the specific experimental procedure are illustrated in the ESI.† The XRD pattern of biochar is shown in Fig. S10.† As revealed in Fig. 6a, there is no peak of NCM in the XRD pattern of gas reduction products, indicating that reducing gases promote the complete decomposition

Transition metals change from high valence states to low valence ones: Ni, Co (+3 → +2 → 0) and Mn (+4 → +2), which can be concluded from the XPS analysis results. After the synergistic reduction effect of gas and biochar, the octahedral lattice structure completely collapses, and then the Ni and Co atoms escape from the oxygen octahedra to form Ni and Co metals. Li element combines with CO₂ to form Li₂CO₃ which is beneficial for recovery in the subsequent leaching process. What is more, due to the strong covalent bond of MnO, it will not undertake reduction reactions with reducing gases or biochar within the temperature range and thus remains stable in the subsequent process.⁵⁹ Finally, the off-gas compositions were analyzed by the TG-DSC-MS test simulating the roasting process (Fig. S12†). It can be seen from Fig. S12† that the roasting process can be divided into three stages: the heating stage, holding stage, and cooling stage. Throughout the gas mass spectra of three stages, the off-gas compositions can be divided into two parts: 1. the gases generated by the reduction reactions of the NCM-523 decomposition products and the carbon combustion reactions (CO₂, CO, and N₂); 2. the unreacted reduction gases (H₂, CH₄, NH₃, and CO).

Optimization of carbonated water leaching

The detailed model construction and verification process are presented in the ESI.† From the statistical analysis results, it can be concluded that the constructed model can be utilized to analyze and predict the carbonated water leaching process, and optimize the leaching conditions.

2D contour plots and 3D surfaces. By plotting the dependent variable as a function of two independent variables and keeping all other variables at fixed levels, the 3D response surfaces can reveal relationships among variables and facilitate intuitive comprehension of the interactions among independent variables. Therefore, 3D response surfaces and 2D contour plots of the measured responses were constructed based on the quadratic function model, presented in Fig. 8 and Fig. S14,† respectively. The independent effects of four variable factors (leaching time, flow rate, temperature, and solid-liquid ratio) and the interactions among the different variables on the leaching rate of Li are displayed in the 3D response surfaces along with the corresponding contour plots. The response surfaces of all factors exhibit a convex shape, which clearly indicates that each independent variable has a unique maximum value, of the optimal solution. In the meantime, the nonlinear nature of 3D response surfaces and contour plots demonstrates that there is no direct linear relationship among the independent variables. As a result, there are considerable interactions between each independent variable and the leaching rate of Li. From Fig. 8a–f, with any two factors fixed, the leaching rates of Li first increase and then decrease with the increase of time, temperature, and flow rate. In contrast, in Fig. 8c, e, and f, the leaching rates of Li decrease with the increase of the solid-liquid ratio under any two fixed factors. This is the reason that a larger solid-liquid ratio means that less LiHCO₃ can be recovered under the same solubility.

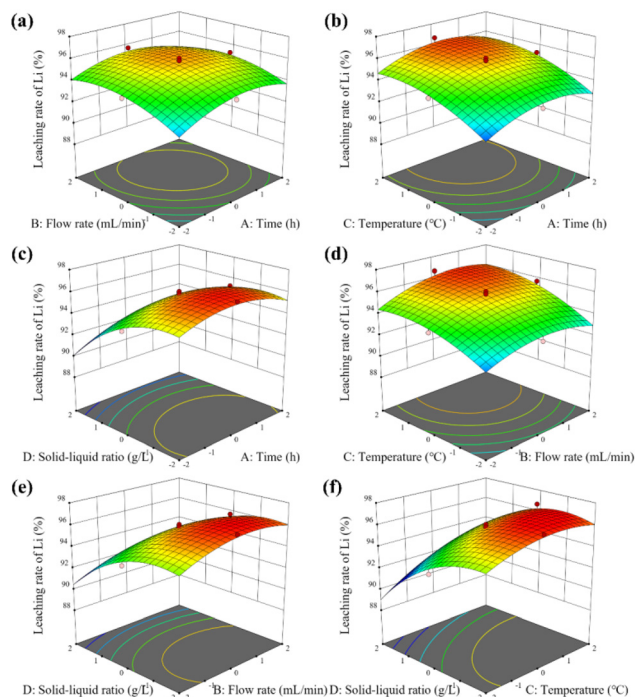


Fig. 8 3D surfaces of the response surface analysis: (a) time and flow rate, (b) time and temperature, (c) time and solid-liquid ratio, (d) flow rate and temperature, (e) flow rate and solid-liquid ratio, and (f) temperature and solid-liquid ratio.

Optimal conditions. An optimized quadratic regression model was analyzed to obtain the maximum leaching rate of Li. The results of the response surface model demonstrated that the optimal conditions for the leaching rate of Li in the carbonated water leaching process are as follows: the time was 3.101 h, the CO₂ flow rate was 137.374 mL min⁻¹, the temperature was 66.667 °C, and the solid-liquid ratio was 24.444 g L⁻¹. Since the optimal leaching conditions do not meet the requirements for the convenience and feasibility of practical operation, the optimized parameters need to be modified appropriately. The modified leaching conditions are as follows: the time was 3.1 h, the CO₂ flow rate was 135 mL min⁻¹, the temperature was 67 °C, and the solid-liquid ratio was 25 g L⁻¹. Under the above conditions, three parallel tests were carried out, and the average leaching rate of Li was 96.83%, which was very close to the response value. To sum up, in this study, a quadratic regression model was reasonably constructed by making use of the RSM and CCD methods, and the model fitting effect was satisfactory. Thence, the selective recovery efficiency of Li during carbonated water leaching was successfully predicted and the enhancement of the overall recovery process was realized.

An enhanced recycling strategy

After the biomass reduction roasting and the carbonated water leaching treatment, the final products were divided into two parts: filter residues and filtrate. Among them, filter residues

mainly include Ni, Co, and MnO. The major component in the filtrate is LiHCO_3 , which can be evaporated and crystallized to obtain Li_2CO_3 in the subsequent recovery process.⁶⁰ The SEM image and XRD pattern of the obtained Li_2CO_3 are shown in Fig. S15.† The diffraction peaks are in good agreement with the characteristic peaks of Li_2CO_3 , indicating that the recovered Li_2CO_3 holds a good crystal structure. The SEM image reveals that the recovered Li_2CO_3 particles are rod-shaped with an average diameter of 2 μm and length of 10 μm . Meanwhile, the purity of the recovered Li_2CO_3 was analyzed by ICP-OES, and the results are listed in Table S7.† The purity as high as 99.79% demonstrates the feasibility of recovering battery-grade Li_2CO_3 (purity > 99.9%) by the enhanced recycling strategy in the future. It is worth noting that the recovery efficiencies (Ni, Co, and Mn) in the filter residues also need to be analyzed by ICP-OES (Fig. S16†). The relatively high recovery efficiencies of these valuable metals indicate that this enhanced recycling strategy accomplishes preferential and efficient recovery of high-purity Li_2CO_3 without the expense of other valuable metals.

With the aim of exploring the industrial application potential of the enhanced recycling strategy, common LIB cathode materials (LCO, NCM, and LMO) were selected and mixed in a certain proportion (the ratio is 1:1:1) to simulate the raw materials of the actual recycling process. Since these lithium transition metal oxides have similar O-cage structures, the selective recovery of Li as well as the separation of valuable metals can theoretically be achieved by the enhanced recovery process.⁵⁹ From the XRD pattern in Fig. 9a, it can be perceived that the mixed materials are composed of LCO, NCM, and LMO without other impurity peaks. After the recovery process under the above optimized conditions, the recovery efficiencies of Li, Ni, Co, and Mn are shown in Fig. 9b. Among them, the recovery efficiency of Li is 96.35%, which is very similar to the recycling of NCM-523 alone, and the recovery efficiencies of Ni, Co, and Mn are all close to 100%. Hence, from the XRD pattern of the roasted products of mixed cathode materials (Fig. 9a), Li is recovered as Li_2CO_3 , and Ni, Co, and Mn elements are converted into metals or metal oxides, which is also consistent with the XRD pattern results of recovering NCM-523 alone. To sum up, the enhanced recovery process which combines pyrometallurgy and hydrometallurgy can not

only be applied to recycle multiple cathode materials, but also offer a new perspective for the selective recovery of Li and the separation of valuable metals in future industrial applications.

Economic assessment

The economic assessment, which is crucial for realizing the industrial application of the designed recycling strategy, was investigated based on the optimized results of the enhanced recycling process. The total costs of the designed recycling process mainly include raw materials (mainly BDs and spent NCM-523), depreciation, the maintenance of the adopted equipment, electric power consumptions, labor, and reagent consumptions (chiefly BDs, water, and CO_2). The energy-consuming equipment in the recovery process includes heat treatment furnaces, heaters, self-discharging filtering machines, multi-stage evaporators, and magnetic separators. Among them, the parameters of the utilized equipment refer to the existing common equipment in other research studies. For recycling 1 ton of spent NCM-523 powder, the qualities, unit prices, and incomes of the products are listed in Table S8;† at the same time, the costs, revenues, and profits are listed in Table S9 (the detailed calculation process is listed in the ESI).† Obviously, the enhanced recycling strategy under the optimal conditions can harvest 71.65 kg of Li_2CO_3 , 326.96 kg of Ni, 126.06 kg of Co, and 174.45 kg of MnO per ton of spent NCM-523 powder, respectively, along with the total revenue of \$19 370.53. With regard to the above-mentioned costs (the total cost of \$1295.86 including $C_{\text{C\&T}}$ and C_{T}), the profits of recycling 1 ton of NCM-523 powder are calculated to be \$18 074.67. Overall, the economic assessment results indicate that the enhanced recycling strategy which combines biomass reduction roasting and carbonated water leaching can operate economically in the long term.

The advantages of utilizing bean dreg

This work was compared with relevant previous references to illuminate the advantages of using BDs as a green reducing agent in the enhanced recycling strategy. The recovery efficiencies of Li, recovery profits, and environmental influences with anode graphite, lignite, coke, and different biomass as reducing agents in the relevant references are summarized in Table S11† for a systematic discussion. Firstly, it can be discovered from Table S11† that the exploitation of BDs as a green reducing agent has the highest recovery efficiency of Li. Secondly, in terms of the recovery profit, the enhanced recycling strategy has relatively high returns. Finally, from the perspective of environmental influence, the utilization of BDs can greatly reduce the emission of CO_2 and other greenhouse gases, indicating that the enhanced recycling strategy is environmentally friendly.

Conclusions

Herein, an enhanced recycling strategy combining biomass reduction roasting and carbonated water leaching is proposed

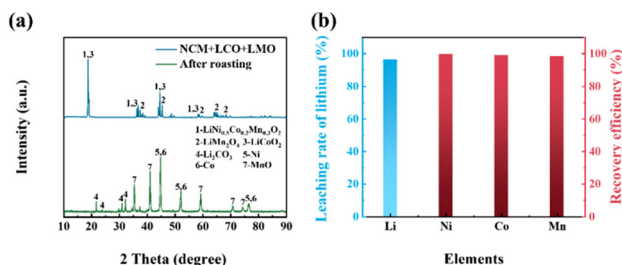


Fig. 9 (a) The XRD patterns of mixed cathode materials and roasted products; (b) the leaching rate of Li and the recovery efficiencies of Ni, Co, and Mn.

to achieve efficient selective recovery of Li. The thermodynamics and TG-DSC-MS analysis results testified that the reducing gases generated by the pyrolysis of the green reducing agent BDs can accelerate the decomposition of NCM-523 by the coupled reaction and lower the roasting temperature. The effect of roasting parameters was systematically studied. Under the optimal conditions of a roasting temperature of 700 °C, a dosage ratio of 1 : 0.3, and a roasting time of 40 min, the roasted products consisted of Li_2CO_3 , Ni, Co, and MnO, and the leaching rate of Li was 93.78%. To explore the thermochemical reaction mechanisms of the roasting process, gas reduction and biochar reduction were investigated, respectively, and the morphologies and chemical compositions of the products after roasting and carbonated water leaching were investigated by SEM, XRD, and XPS. It can be concluded from the analysis results that under the synergistic reduction effect of gas and biochar, the covalent bonds of the oxygen octahedral lattices in NCM-523 are broken, resulting in the release of transition metals and Li. With the purpose of further enhancing the recycling process, the variables in carbonated water leaching (time, CO_2 flow rate, temperature, solid-liquid ratio) were optimized by the RSM and CCD methods. Under the optimized conditions, the average leaching rate of Li from parallel tests was 96.83%, which was very close to the response value. Finally, through full cost accounting and economic assessment, it is justified that this strategy owned high recovery profits and practical application feasibility. In conclusion, the enhanced recycling strategy based on the pyrolysis of BDs can not only be applied to effectively recover high-purity Li_2CO_3 , but also offer a new perspective and great development potential for the future industrial recycling of the spent LIBs.

Author contributions

Tianning Lin: performed the experiment, data collection and analysis, and writing of the manuscript. Yue Wang: conceptualization, methodology and formal analysis. Shan Jin and Deying Mu: product analysis and sample characterization. Jian Zhang and Jianquan Liang: result analysis and review. Changsong Dai: funding acquisition, supervision, and writing – review.

Conflicts of interest

There are no conflicts to declare.

Acknowledgements

This work was finally supported by the National Natural Science Foundation of China (NSFC Grants 52074098), the State Grid Heilongjiang Electric Power Co., Ltd, Technology Project Funding (power lithium-ion battery gradient utilization and resourceful recycling and re-preparation research,

522437200034), and the Foundation of Key Program of Sci-Tech Innovation in Ningbo (2019B10114).

References

- 1 Y. Liang, C. Z. Zhao, H. Yuan, Y. Chen, W. Zhang, J. Q. Huang, D. Yu, Y. Liu, M. M. Titirici, Y. L. Chueh, H. Yu and Q. Zhang, *InfoMat*, 2019, **1**, 6–32.
- 2 G. Harper, R. Sommerville, E. Kendrick, L. Driscoll, P. Slater, R. Stolkin, A. Walton, P. Christensen, O. Heidrich, S. Lambert, A. Abbott, K. Ryder, L. Gaines and P. Anderson, *Nature*, 2019, **575**, 75–86.
- 3 E. Fan, L. Li, Z. Wang, J. Lin, Y. Huang, Y. Yao, R. Chen and F. Wu, *Chem. Rev.*, 2020, **120**, 7020–7063.
- 4 S. Natarajan, M. L. Divya and V. Aravindan, *J. Energy Chem.*, 2022, **71**, 351–369.
- 5 A. K. Awasthi and J. Li, *Resour., Conserv. Recycl.*, 2017, **126**, 228–239.
- 6 H. Wang, K. Huang, Y. Zhang, X. Chen, W. Jin, S. Zheng, Y. Zhang and P. Li, *ACS Sustainable Chem. Eng.*, 2017, **5**, 11489–11495.
- 7 S. Jin, D. Mu, Z. Lu, R. Li, Z. Liu, Y. Wang, S. Tian and C. Dai, *J. Cleaner Prod.*, 2022, **340**, 130585.
- 8 Y. Guo, F. Li, H. Zhu, G. Li, J. Huang and W. He, *Waste Manage.*, 2016, **51**, 227–233.
- 9 Y. Yang, E. G. Okonkwo, G. Huang, S. Xu, W. Sun and Y. He, *Energy Storage Mater.*, 2021, **36**, 186–212.
- 10 P. Meshram, A. Mishra, Abhilash and R. Sahu, *Chemosphere*, 2020, **242**, 125291.
- 11 Y. Wang, N. An, L. Wen, L. Wang, X. Jiang, F. Hou, Y. Yin and J. Liang, *J. Energy Chem.*, 2021, **55**, 391–419.
- 12 J. Zhao, X. Qu, J. Qu, B. Zhang, Z. Ning, H. Xie, X. Zhou, Q. Song, P. Xing and H. Yin, *J. Hazard. Mater.*, 2019, **379**, 120817.
- 13 A. M. Bernardes, D. C. R. Espinosa and J. A. S. Tenório, *J. Power Sources*, 2004, **130**, 291–298.
- 14 B. Makuza, Q. Tian, X. Guo, K. Chattopadhyay and D. Yu, *J. Power Sources*, 2021, **491**, 229622.
- 15 Y. Chen, N. Liu, F. Hu, L. Ye, Y. Xi and S. Yang, *Waste Manage.*, 2018, **75**, 469–476.
- 16 O. Dolotko, I. Z. Hlova, Y. Mudryk, S. Gupta and V. P. Balema, *J. Alloys Compd.*, 2020, **824**, 153876.
- 17 F. Meng, J. McNeice, S. S. Zadeh and A. Ghahreman, *Miner. Process. Extr. Metall. Rev.*, 2019, **42**, 123–141.
- 18 D. J. Garole, R. Hossain, V. J. Garole, V. Sahajwalla, J. Nerkar and D. P. Dubal, *ChemSusChem*, 2020, **13**, 3079–3100.
- 19 N. J. Boxall, K. Y. Cheng, W. Bruckard and A. H. Kaksonen, *J. Hazard. Mater.*, 2018, **360**, 504–511.
- 20 S. Xiao, G. Ren, M. Xie, B. Pan, Y. Fan, F. Wang and X. Xia, *J. Sustain. Metall.*, 2017, **3**, 703–710.
- 21 X. Sun, M. Ouyang and H. Hao, *Joule*, 2022, **6**, 1738–1742.
- 22 W. Yu, Y. Guo, Z. Shang, Y. Zhang and S. Xu, *eTransportation*, 2022, **11**, 100155.

- 23 J. Xiao, J. Li and Z. Xu, *Environ. Sci. Technol.*, 2020, **54**, 9–25.
- 24 J. Yang, Y. Chen, Y. Li, X. Xi, J. Zheng, Y. Zhu, Y. Xiong and S. Liu, *ACS Appl. Mater. Interfaces*, 2021, **13**, 25981–25992.
- 25 V. Chandran, A. Ghosh, C. K. Patil, V. Mohanavel, A. K. Priya, R. Rahim, R. Madavan, U. Muthuraman and A. Karthick, *Mater. Today: Proc.*, 2021, **47**, 167–180.
- 26 T. Georgi-Maschler, B. Friedrich, R. Weyhe, H. Heegn and M. Rutz, *J. Power Sources*, 2012, **207**, 173–182.
- 27 J. Xiao, J. Li and Z. Xu, *J. Hazard. Mater.*, 2017, **338**, 124–131.
- 28 J. Li, G. Wang and Z. Xu, *J. Hazard. Mater.*, 2016, **302**, 97–104.
- 29 P. Xu, C. Liu, X. Zhang, X. Zheng, W. Lv, F. Rao, P. Yao, J. Wang and Z. Sun, *ACS Sustainable Chem. Eng.*, 2021, **9**, 2271–2279.
- 30 Y. Tang, H. Xie, B. Zhang, X. Chen, Z. Zhao, J. Qu, P. Xing and H. Yin, *Waste Manage.*, 2019, **97**, 140–148.
- 31 Y. Zhao, B. Liu, L. Zhang and S. Guo, *J. Hazard. Mater.*, 2020, **384**, 121487.
- 32 A. V. Bridgwater, *Biomass Bioenergy*, 2012, **38**, 68–94.
- 33 T. Y. A. Fahmy, Y. Fahmy, F. Mobarak, M. El-Sakhawy and R. E. Abou-Zeid, *Environ. Dev. Sustain.*, 2018, **22**, 17–32.
- 34 X. Hu and M. Gholizadeh, *J. Energy Chem.*, 2019, **39**, 109–143.
- 35 F. Wang, D. Ouyang, Z. Zhou, S. J. Page, D. Liu and X. Zhao, *J. Energy Chem.*, 2021, **57**, 247–280.
- 36 Y. Li, B. Xing, Y. Ding, X. Han and S. Wang, *Bioresour. Technol.*, 2020, **312**, 123614.
- 37 F. Zhou, X. Qu, Y. Wu, J. Zhao, S. Gao, D. Wang and H. Yin, *ACS Sustainable Chem. Eng.*, 2022, **10**, 1287–1297.
- 38 X. Chen, Y. Wang, S. Li, Y. Jiang, Y. Cao and X. Ma, *Chem. Eng. J.*, 2022, **434**, 134542.
- 39 G. Zhu, X. Zhu, Z. Xiao, R. Zhou and F. Yi, *Waste Manage.*, 2012, **32**, 2287–2293.
- 40 S. Xue, X. Zhang, H. H. Ngo, W. Guo, H. Wen, C. Li, Y. Zhang and C. Ma, *Bioresour. Technol.*, 2019, **292**, 121927.
- 41 X. Wu, G. Lei, Y. Xu and H. Liu, *J. Mater. Sci.: Mater. Electron.*, 2019, **31**, 728–739.
- 42 W. Lu, Y. Zhang, C. Xiao, D. Chen, Q. Ye, C. Zhang, X. Meng and S. Wang, *Foods*, 2022, **11**, 1475.
- 43 L. Xing, S. Lin and J. Yu, *Ind. Eng. Chem. Res.*, 2021, **60**, 10303–10311.
- 44 L.-P. He, S.-Y. Sun, Y.-Y. Mu, X.-F. Song and J.-G. Yu, *ACS Sustainable Chem. Eng.*, 2016, **5**, 714–721.
- 45 L. Li, J. Ge, F. Wu, R. Chen, S. Chen and B. Wu, *J. Hazard. Mater.*, 2010, **176**, 288–293.
- 46 X. Chen, C. Luo, J. Zhang, J. Kong and T. Zhou, *ACS Sustainable Chem. Eng.*, 2015, **3**, 3104–3113.
- 47 L. Li, J. Lu, Y. Ren, X. X. Zhang, R. J. Chen, F. Wu and K. Amine, *J. Power Sources*, 2012, **218**, 21–27.
- 48 S. Soleimanpour, S. M. Sadrameli, S. A. H. S. Mousavi and M. Jafaripour, *J. Energy Storage*, 2022, **45**, 103735.
- 49 Y. Zhao, B. Liu, L. Zhang and S. Guo, *J. Hazard. Mater.*, 2020, **396**, 122740.
- 50 B. Makuza, D. Yu, Z. Huang, Q. Tian and X. Guo, *Resour. Conserv. Recycl.*, 2021, **174**, 105784.
- 51 Y. Zhang, W. Wang, Q. Fang and S. Xu, *Waste Manage.*, 2020, **102**, 847–855.
- 52 C. Yang, J. Zhang, Z. Cao, Q. Jing, Y. Chen and C. Wang, *ACS Sustainable Chem. Eng.*, 2020, **8**, 15732–15739.
- 53 L. Deng, Z. Xu, M. Wang, H. Shentu, X. Liu, J. Xiong, Y.-J. Cheng, C. Wang, M. Zhou, J. Gao and Y. Xia, *Green Chem.*, 2022, **24**, 779–789.
- 54 G. Jiang, Y. Zhang, Q. Meng, Y. Zhang, P. Dong, M. Zhang and X. Yang, *ACS Sustainable Chem. Eng.*, 2020, **8**, 18138–18147.
- 55 L. Riekehr, J. Liu, B. Schwarz, F. Sigel, I. Kerkamm, Y. Xia and H. Ehrenberg, *J. Power Sources*, 2016, **306**, 135–147.
- 56 J. Mao, J. Li and Z. Xu, *J. Cleaner Prod.*, 2018, **205**, 923–929.
- 57 E. Lee, K.-R. Lee and B.-J. Lee, *Comput. Mater. Sci.*, 2018, **142**, 47–58.
- 58 J. Xiao, B. Niu and Z. Xu, *J. Hazard. Mater.*, 2021, **418**, 126319.
- 59 J. Safarian, G. Tranell, L. Kolbeinsen, M. Tangstad, S. Gaal and J. Kaczorowski, *Metall. Mater. Trans. B*, 2008, **39**, 702–712.
- 60 J. Zhang, J. Hu, W. Zhang, Y. Chen and C. Wang, *J. Cleaner Prod.*, 2018, **204**, 437–446.